Supplement of Earth Surf. Dynam., 7, 191–197, 2019
https://doi.org/10.5194/esurf-7-191-2019-supplement

Earth Surface Dynamics
Open Access
EGU

Supplement of

Aging of basalt volcanic systems and decreasing CO_2 consumption by weathering

Janine Börker et al.

Correspondence to: Janine Börker (janine.boerker@uni-hamburg.de), Jens Hartmann (geo@hattes.de)

Supplementary information

Supplemental Material A to G describe available information on the used volcanic, basalt dominated areas and the calculation procedures. For the active volcanic fields (AVF) a detailed description of the calculation for the fraction of the Holocene area on the total area is given. Additionally, a description of the newly introduced alkalinity flux scaling law for young active basaltic areas and for the calculation of the global fluxes is provided.

Supplemental Material A: Summary of data compilation as applied in the main text

Supplemental Material B: New data for active volcanic fields as described in Table S1, in addition to Li et al. (2016)

Supplemental Material C: Saturation state with respect to calcite

Supplemental Material D: Additional relations between Alkalinity, Reactivity and Holocene area fraction

Supplemental Material E: Estimation of the parameters for the new scaling law

Supplemental Material F: Global calculations CO_2 consumption by basalt weathering

Supplemental Material G: Enhanced global basalt map beyond GLIM

Supplemental Material A: Summary of data compilation as applied in the main text

Table S1: *Summary of the data of Inactive Volcanic Fields (IVFs) and Active Volcanic Fields (AVFs) used for the analysis in the main text (Li et al., 2016), as well as calculated Holocene fraction and Reactivity R.*

No.	Name	Volcanic activity	T (°C)	σ_T	Runoff (mm/yr)	σ_{Runoff}	Alkalinity (μmol/L)	$\sigma_{Alkalinity}$	Alkalinity flux rate (10^6 mol/km^2/yr)	$\sigma_{Alkalinity\ flux\ rate}$	Latitude (°)	Longitude (°)	Holocene fraction (%)	Calculated Reactivity R
1	Massif Central	Inactive	8.70	0.65	406	20	916	46	0.372	0.026	45.7700	2.9600	0	0.96
2	South Africa	Inactive	12.70	1.80	244	55	1728	1078	0.420	0.130	-25.2758	29.6324	0	0.85
3	Karelia	Inactive	-2.00	1.00	285	20	460	41	0.131	0.007	65.0000	31.0000	0	0.64
4	Coastal Deccan	Inactive	25.10	0.50	1690	150	657	17	1.110	0.103	16.9300	73.5100	0	1.07
5	Interior Deccan	Inactive	25.40	0.50	401	48	2839	170	1.138	0.152	21.0000	74.0000	0	1.08
6	Siberian Traps	Inactive	-8.50	0.65	254	25	501	89	0.127	0.019	65.0000	100.0000	0	0.92
7	Mt. Emei	Inactive	6.20	1.00	1350	75	238	23	0.321	0.036	27.4462	103.3255	0	0.96
8	Leiqiong	Inactive	24.00	1.00	797	100	1923	165	1.532	0.233	20.4600	110.1800	0	1.58
9	Nanjing	Inactive	15.20	1.00	330	48	1595	63	0.526	0.079	32.7400	118.3900	0	0.92
10	Xiaoxinganling	Inactive	-1.00	1.00	243	50	1065	132	0.259	0.062	49.0942	128.1704	0	1.19
11	Tumen River	Inactive	-4.00	2.00	273	50	763	50	0.208	0.041	42.5000	128.5000	0	1.15
12	Mudan River	Inactive	3.20	2.00	209	46	977	87	0.204	0.048	43.7500	128.7200	0	0.73
13	Southeast Australia	Inactive	13.00	0.10	74	14	5956	657	0.441	0.097	-38.1883	142.8587	0	0.88
14	Tasmania	Inactive	10.10	0.25	221	30	1704	437	0.377	0.109	-42.1900	146.7600	0	0.89
15	North Island, NZ	Inactive	13.00	2.00	920	161	478	131	0.439	0.143	-38.0000	176.0000	0	0.88
16	Kauai, Hawaii	Inactive	21.58	0.65	1747	539	588	251	1.026	0.303	22.0000	-159.5000	0	1.22
17	Columbia Plateau	Inactive	7.40	2.00	204	191	927	215	0.189	0.060	44.0000	-118.5000	0	0.53
18	Northeast America	Inactive	0.70	2.30	507	129	465	316	0.235	0.075	47.0483	-75.3229	0	0.98
19	Madeira Island	Inactive	13.50	1.50	1065	100	580	43	0.618	0.074	32.8000	-17.0000	0	1.19
20	Easter Island	Active	20.60	1.00	580	100	1306	132	0.757	0.151	-27.1200	-109.3700	3.36	0.96
21	Mt. Cameroon	Active	14.00	2.00	2120	500	2368	110	5.020	1.207	4.0000	9.0000	96.57	9.42
22	Mt. Etna	Active	14.90	0.20	640	80	9286	539	5.943	0.819	37.7514	14.9974	79.56	10.57

23	Virunga	Active	20.80	1.30	1709	380	2646	1757	4.522	2.110	-1.5000	29.5000	47.95	5.64
24	La Réunion	Active	17.00	2.00	1712	652	1243	290	2.127	0.031	-21.1200	55.5400	27.73	3.33
25	Wudalianchi Lake	Active	-1.00	1.00	243	50	1919	190	0.466	0.106	48.7010	126.1411	14.82	2.15
26	Japan	Active	10.99	1.12	1236	64	584	73	0.722	0.107	35.9234	135.3560	8.7	1.62
27	Kamchatka	Active	-3.50	2.00	520	50	854	100	0.444	0.067	55.0000	159.0000	2.28	2.38
28	Taranaki	Active	10.00	3.00	1296	223	667	34	0.864	0.155	-39.3000	174.0000	8	2.06
29	Big Island, Hawaii	Active	15.44	2.00	935	269	951	424	0.889	0.303	19.5000	-155.5000	14.08	1.53
30	High Cascades	Active	6.81	0.47	382	172	776	175	0.296	0.108	45.1924	-121.6844	0.2	0.86
31	Iceland	Active	0.70	0.65	1734	136	498	74	0.864	0.109	65.0000	-18.0000	13.19	3.60
32	São Miguel Island	Active	16.00	1.00	879	50	2331	200	2.047	0.211	37.7700	-25.5000	9.35	3.41
33	Tianchi Lake	Active	-7.30	2.00	291*	100	2445	300	0.711	0.260	42.0000	128.0500	65.34	4.79

**The runoff for Tianchi Lake was recalculated after Fekete et al. (2002).*

Supplemental Material B: New data for active volcanic fields as described in Table S1, in addition to Li et al. (2016)

In the following, all active volcanic provinces used for this study are described. Note, that for all inactive fields a detailed description of the input data can be found in Li et al. (2016), as well as the origin of the temperature, runoff and alkalinity/DIC concentration data for active and inactive volcanic fields. If watersheds are considered for the calculations of the Holocene area, they are based on the locations of the sampling points (see Li et al. (2016)).

For the calculation of the Holocene fraction area for each volcanic field, based on mapped basic volcanic rocks only (e.g., “vb” in the GLiM), we used several time spans. A polygon with an age description of Holocene (0-11.7 ka) was classified as a “Holocene”-area. If a polygon had an age description, which laid in the time interval of 0 to 2.58 Ma, but it was not clearly defined as of Holocene or Pleistocene age, we defined it as “Quaternary” and applied a theoretical Holocene fraction by the ratio of Holocene time span and Quaternary time span. All other polygons with age descriptions older than Holocene and not defined as “Quaternary” were defined as “non-Holocene”.

Numbers behind a region indicate the number in the summary table S1.

Easter Island (No.20)

Easter Island is a volcanic island in the eastern Pacific. Its volcanic nature is related to the Easter Island Hotspot. The geologic map used for this study was digitized after a map of Gioncada et al. (2010) and references therein. The island is composed mostly of hawaiites, mugearites and olivine basalts and it comprises volcanic ages from 3 Ma to recent. The different age classifications and lithologies are listed in the table below. Due to the precise age information the rocks are directly classified into Holocene rocks and non-Holocene rocks. The total basaltic area of the island is 162.27 km^2, the Holocene area 5.45 km^2 and the non-Holocene area 156.82 km^2, resulting in a Holocene area fraction of 3.36%.

Table S2: *Classification of the map data of Easter Island. The first three columns provide the original map data, whereas the column "System/Series" shows our interpretation of the map data.*

Name	Description	Age	System/Series
TE1	Terevaka, hawaiites and olivine basalts	0.3-1.9 Ma	non-Holocene
TE2	Terevaka, hawaiites and olivine basalts	0.3-1.9 Ma	non-Holocene
TE3	Terevaka, hawaiites and olivine basalts	0.3-1.9 Ma	non-Holocene
HH2	Anakena, Hiva-Hiva, hawaiites and olivine basalts	0-2,000 a ago	Holocene
RA1	Rano Aroi, hawaiites, olivine basalts and mugearites	0.2 Ma	non-Holocene
RA5	Rano Aroi, hawaiites, olivine basalts and mugearites	0.2 Ma	non-Holocene
RA4	Rano Aroi, hawaiites, olivine basalts and mugearites	0.2 Ma	non-Holocene
RA2	Rano Aroi, hawaiites, olivine basalts and mugearites	0.2 Ma	non-Holocene
RA8	Rano Aroi, hawaiites, olivine basalts and mugearites	0.2 Ma	non-Holocene
RA7	Rano Aroi, hawaiites, olivine basalts and mugearites	0.2 Ma	non-Holocene
RA6	Rano Aroi, hawaiites, olivine basalts and mugearites	0.2 Ma	non-Holocene
RA3	Rano Aroi, hawaiites, olivine basalts and mugearites	0.2 Ma	non-Holocene
HH1	Anakena, Hiva-Hiva, hawaiites and olivine basalts	0-2,000 a ago	Holocene
PO2	Polke, alkali basalts, hawaiites to mugearites	0.61-3 Ma	non-Holocene

PO1	Polke, alkali basalts, hawaiites to mugearites	0.61-3 Ma	non-Holocene
PO5	Polke, alkali basalts, hawaiites to mugearites	0.61-3 Ma	non-Holocene
PO4	Polke, alkali basalts, hawaiites to mugearites	0.61-3 Ma	non-Holocene
TR	Maunga Orito, rhyolite; Maunga Parehe, trachyte	not known	not considered
PO3	Polke, alkali basalts, hawaiites to mugearites	0.61-3 Ma	non-Holocene
RK1	Rano Kau, alkali basalts, hawaiites to benmoreites	0.2-2.5 Ma	non-Holocene
RK2	Rano Kau, alkali basalts, hawaiites to benmoreites	0.2-2.5 Ma	non-Holocene
TA4	Tangaroa, hawaiites, olivine basalts and mugearites	0.2 Ma	non-Holocene
TA1	Tangaroa, hawaiites, olivine basalts and mugearites	0.2 Ma	non-Holocene
TA2	Tangaroa, hawaiites, olivine basalts and mugearites	0.2 Ma	non-Holocene
TA6	Tangaroa, hawaiites, olivine basalts and mugearites	0.2 Ma	non-Holocene
TA3	Tangaroa, hawaiites, olivine basalts and mugearites	0.2 Ma	non-Holocene
TA5	Tangaroa, hawaiites, olivine basalts and mugearites	0.2 Ma	non-Holocene
TA7	Tangaroa, hawaiites, olivine basalts and mugearites	0.2 Ma	non-Holocene

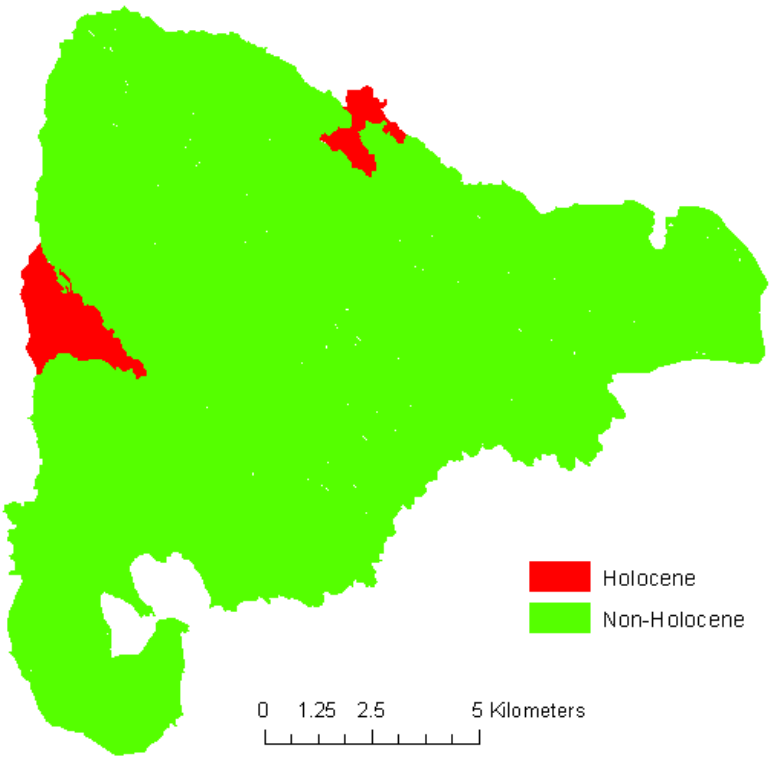

Figure S1: *Map of Easter Island showing the Holocene and non-Holocene areas.*

Table S3: *Calculated areas for Easter Island. The Holocene fraction is derived by the ratio of Holocene area/Total area.*

Area Holocene (km^2)	Area Non-Holocene (km^2)	Area Quaternary (km^2)	Total Area (km^2)	Holocene (%)
5.45	156.82	0	162.27	3.36

Mount Cameroon (No.21)

Mount Cameroon is part of a volcanic chain at the coast of West Africa. The geological map was digitized from Le Maréchal (1975). The location of the sampling points were derived from Benedetti et al. (2003). The age classification (see table below) results in a Holocene fraction of 96.57%.

Table S4: *Classification of the surface ages of Mt. Cameroon. Note that the first three columns display the original map data, the column "System/Series" provides the authors interpretation.*

Name	Description	Age	System/Series
beta1	Séries inférieures: basaltes parfois andésitiques sous forme de coulées et de dykes	Oligocene-Eocene	non-Holocene
beta3	Séries supérieures: basaltes parfois andésitiques sous forme de coulées et cinérites	quatenaire récente	Holocene

The interpretation of the ages of Mount Cameroon was difficult, since the ages are not well determined (Ateba et al., 2009). Le Maréchal (1976) describes the ages of the basalts, as well as an unpublished map in Ateba et al. (2009) that shows "young basalts" in the center of Mount Cameroon so that we assumed an age of "recent Quaternary" for "beta3".

Table S5: *Area calculation of Mt. Cameroon. The Holocene fraction is derived by the ratio of Holocene area/Total area.*

Area Holocene (km^2)	Area non-Holocene (km^2)	Area Quaternary (km^2)	Total Area (km^2)	Holocene (%)
1,112.63	39.48	0	1,152.11	96.57

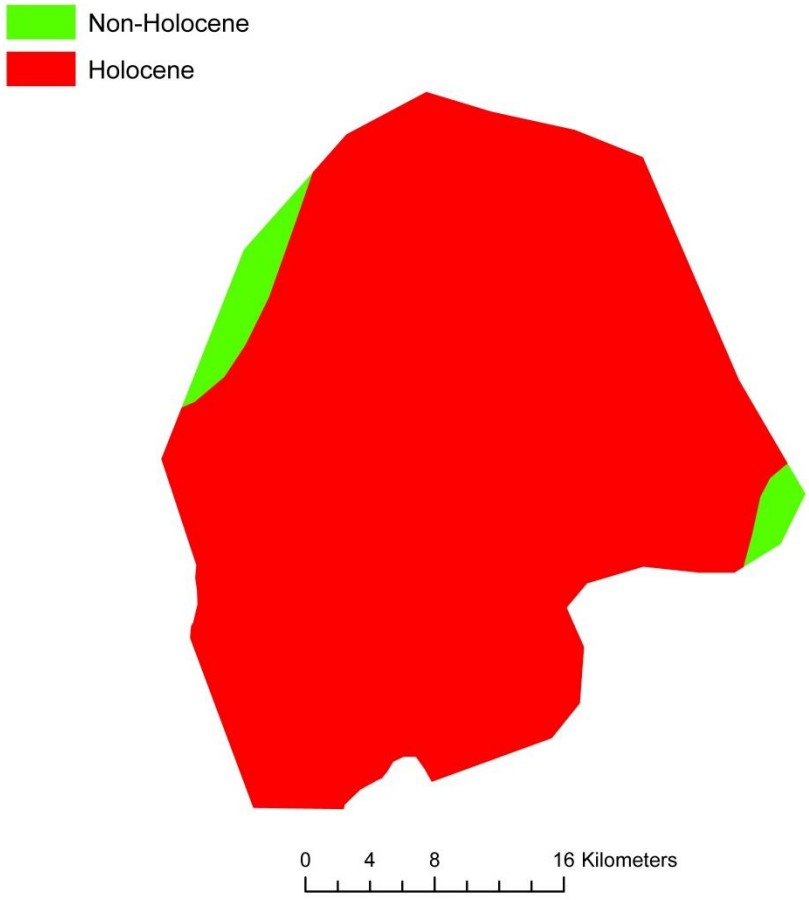

Figure S2: *Map of Mount Cameroon showing the Holocene and non-Holocene area.*

Mount Etna (No.22)

Mount Etna is located at a subduction zone in Italy. Its geological map was digitized from Branca et al. (2011a) and is described in Branca et al. (2011b). The detailed description of the lithologies is shown below and allows for a classification into Holocene, non-Holocene and Quaternary.

The Quaternary rocks are of an age of 3.9 ka to 15 ka, so that they have a time span of 11.1 ka. 7.8 ka is within the Holocene period (3.9 ka to 11.7 ka) considering the Holocene time period going from 0 to 11.7 ka. The fraction of Holocene coverage was than calculated by:

$$Holocene\ fraction = \frac{Area\ Holocene + \left(Area\ Quaternary * \left(\frac{7.8}{11.1}\right)\right)}{Total\ Area}$$

resulting in a Holocene fraction area of 79.56%.

Table S6: *Classification of Etna basaltic rocks showing the original map data (first four columns) and our interpretation of the data ("System/Series").*

Symbol	Name	Description	Age	System/Series
26u	Lava flows, cinder cones and bastions, and fall deposits	basaltic to benmoreitic	122 b.C. – 4 ka	Holocene
27-1	Castings, cinder cones and bastions, and fall deposits	basaltic to mugearitica	1669 - 122 b.C.	Holocene
27-2	Castings, cinder cones and bastions, and fall deposits	basaltic to mugearitica	1971 - 1669	Holocene
27-3	Lava flows, cinder cones and bastions, and fall deposits	basaltic to mugearitica	current - 1971	Holocene
CB26u	Cono e bastione di scorie			Holocene
CB27-1	Cono e bastione di scorie			Holocene
CB27-2	Cono e bastione di scorie			Holocene
CB27-3	Cono e bastione di scorie			Holocene
10a	Intercalated flows in a powerful pyroclastic flow deposit	mugearitica	nn	non-Holocene
14	Succession of alternating flows in pyroclastic deposits	hawaiitica to mugearitica	nn	non-Holocene
15	Flows intercalated with clastic deposits	mugearitica to benmoreitic	nn	non-Holocene
17	Casting interbedded with clastic deposits	benmoreite	nn	non-Holocene
18	Flows	mugearitica-benmoreitic	nn	non-Holocene

18a	Bodies subvulcanici materials come from lavas	mugearitica-benmoreitic	nn	non-Holocene
1a	Bodies subvolcanici		nn	non-Holocene
21b	Porfirichi flows	hawaiitica to mugearitica	nn	non-Holocene
22b	Casting succession	hawaiitica	nn	non-Holocene
24	Of breccia autoclastic often altered to hydrothermalism, associated with lava flows	benmoreitic	nn	non-Holocene
26b	Deposit of debris avalanche monogenic, formed by lava mugearitica blocks	nn	nn	Quaternary
3b	Massive lava flows	basaltic	nn	non-Holocene
1	Underwater transitional composition of volcanics in tholeiitica consist of pillow lavas	tholeiitica	496.1 - 542.2 ka	non-Holocene
10b	Flows intercalated with breccias autoclastic and deposits epiclastici	hawaiitica to mugearitica	101.9ka	non-Holocene
11	Brecce autoclastic and deposits epiclastici	benmoreitic	99.1 - 107.2 ka	non-Holocene
12	Deposits associated with pyroclastic flows	mainly mugearitica	99.9 - 101.8 ka	non-Holocene
13	Castings and slag deposits	hawaiitica	93.0 ka	non-Holocene
14a	Subvulcanici bodies formed by lava massive	mugearitica	85.3 ka	non-Holocene
16	Casting intercalated with thin epiclastici deposits	mugearitica to benmoreitic	85.6 ka	non-Holocene
19	Thin flows to the base, followed by a thick succession pyroclastic	mugeraitica	70.2 - 79.6 ka	non-Holocene
2	Lava flows	tholeiitica	332.4 ka	non-Holocene
20	Fall and pyroclastic flow deposits	hawaiitica to benmoreitic	41.3 - 56.6 ka	non-Holocene
21a	Massive flows and autoclastic interbedded with breccia deposits	hawaiitica to mugearitica	29.1-32.5 ka	non-Holocene
22	Castings, scoria cones and fall deposits	hawaiitica to benmoreitic	28.7-42.1 ka	non-Holocene
25b	Reomorfiche flows	benmoreitic	15.0 - 15.4 ka	non-Holocene
2a	Subvolcanico body structure		320.0 ka	non-Holocene
3a	Strongly altered lava flows	basaltic	180.2 ka	non-Holocene
4a	Massive lava flows	basaltic to mugearitica	129.9 - 154.9 ka	non-Holocene
4b	Thin lava flows	basaltic to mugearitica	134.2 ka	non-Holocene

6	Lave cataclasate	basaltic to mugearitica	128.7 ka	non-Holocene
7	Succession Lava	mugearitica	126.4 ka	non-Holocene
8	Succession lava with thin interbedded deposits epiclastici	hawaiitica to mugearitica	111.9 - 121.2 ka	non-Holocene
9	Lava flows interbedded with massive deposits of local epiclastici	hawaiitica to benmoreitic	105.8 ka	non-Holocene
CB2	Cono e bastione di scorie			non-Holocene
CB22	Cono e bastione di scorie			non-Holocene
CB3a	Cono e bastione di scorie			non-Holocene
CB7	Cono e bastione di scorie			non-Holocene
26l	Lava flows, cinder cones and bastions, and fall deposits	basaltic to benmoreitic	4 - 15ka	Quaternary
CB26l	Cono e bastione di scorie			Quaternary

Table S7: *Table showing the calculated areas for Mount Etna. Note that the Holocene fraction is calculated by the above-mentioned equation considering Holocene area, Quaternary area and total area.*

Area Holocene (km^2)	**Area non-Holocene (km^2)**	**Area Quaternary (km^2)**	**Total Area (km^2)**	**Holocene (%)**
636.16	123.90	338.39	1,098.45	79.56

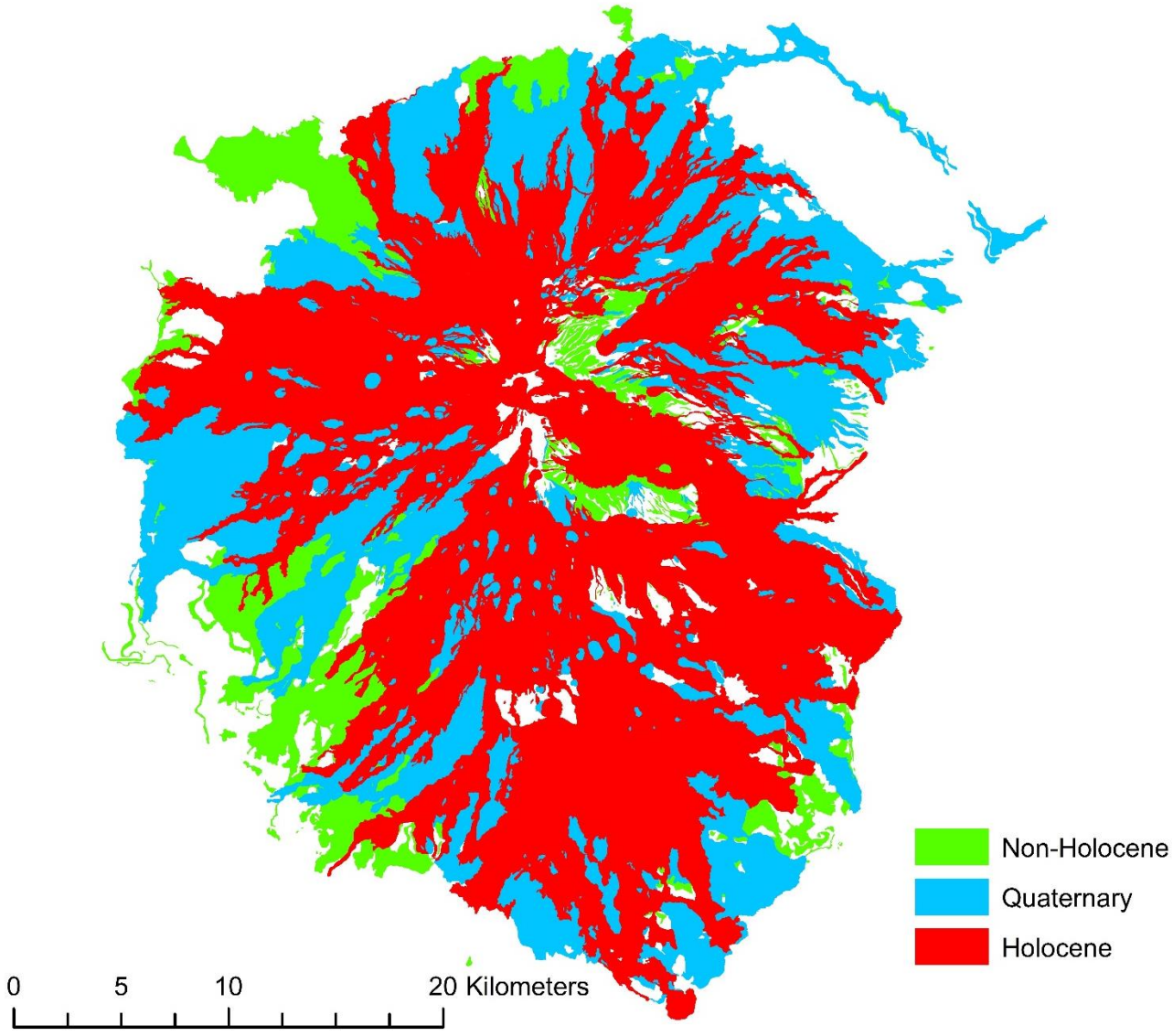

Figure S3: *Map of Etna volcano showing the age distribution of basaltic rocks.*

Virunga (No.23)

The Virunga Volcanic province is located in eastern central Africa and is related to the East African Rift system. The geologic map of this area was compiled from four different maps published by Antun et al. (1971), De Mulder et al. (1986), Smets et al. (2010) and Balagizi et al. (2015).

We assume that the volcanic areas of Nyiragongo and Nyamuragira are of Holocene age, since they are classified as Africa's most active volcanoes, and erupted frequently in the past (Smets et al., 2010; Balagizi et al., 2015). The remaining volcanoes are assumed to be of quaternary age (not older than Pleistocene according to Antun et al. (1971)). For the northeastern part of the map the surface age could not be determined clearly, and was therefore defined as "not known", and included in the calculations as "non-Holocene".

Considering that the Quaternary age period ranges from 0 to 2.58 Ma, the Holocene percentage of the Quaternary area is calculated by the ratio of 11,700 a / 2,580,000 a. The total theoretical Holocene areal percentage is 47.95% using:

$$Holocene\ fraction = \frac{Area\ Holocene + \left(Area\ Quaternary * \left(\frac{11{,}700}{2{,}580{,}000}\right)\right)}{Total\ area}$$

Table S8: *Classification of basaltic rocks in the Virunga province showing the individual volcanoes and our interpretation of their age.*

Id	Volcano	System/Series
0	Nyiragongo	Holocene
1	Nyamuragira	Holocene
2	Muhabura	Quaternary
3	Gahinga	Quaternary
4	Synabaye	Quaternary
5	Bisoke-Sabinyo	Quaternary
6	Bisoke-Sabinyo	Quaternary
7	Bisoke-Sabinyo	Quaternary
8	Karisimbi	Quaternary
9	Remaining areas	not known

Table S9: *Calculated areas for Virunga province. The Holocene fraction is derived by applying the above-mentioned equation considering the Holocene area, Quaternary area and total area.*

Area Holocene (km^2)	Area Non-Holocene (km^2)	Area Quaternary (km^2)	Total Area (km^2)	Holocene (%)
1,518.62	791.26	865.16	3,175.04	47.95

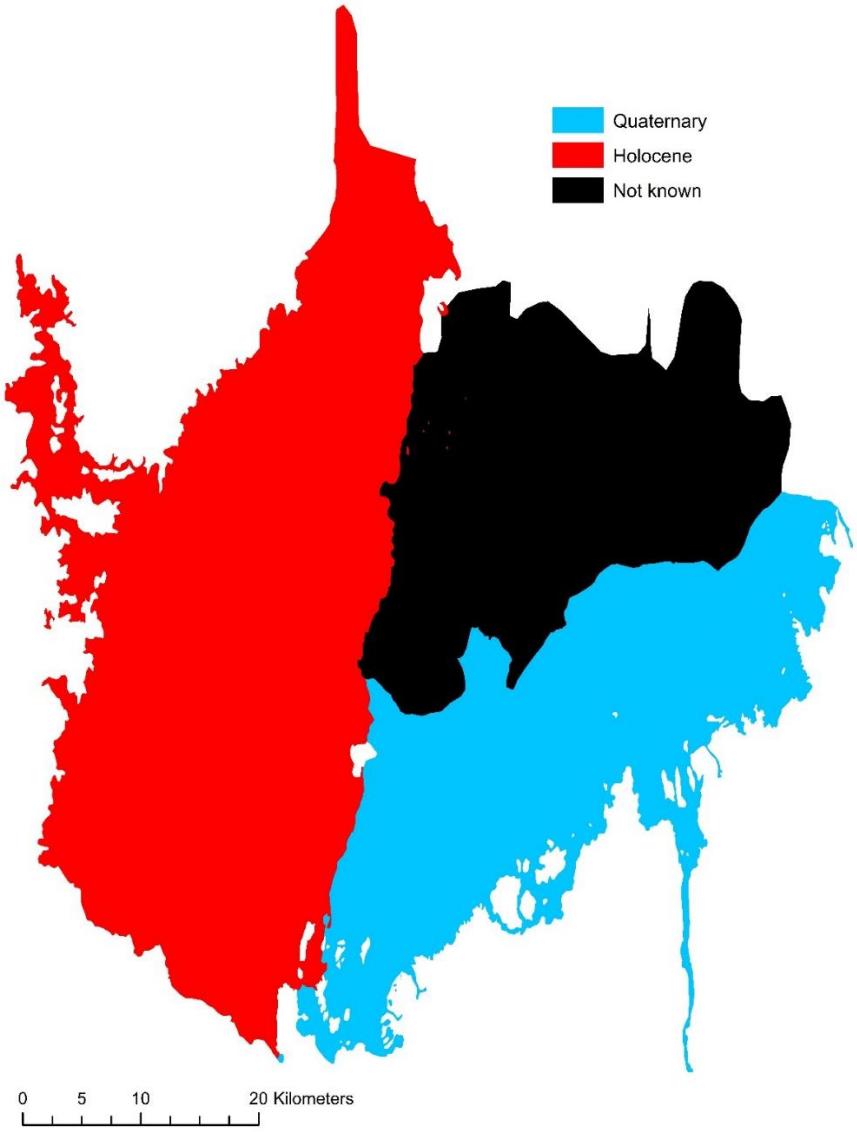

Figure S4: *Map of the Virunga province showing the different areas of basalt classified after age.*

La Réunion (No.24)

The volcanic island La Réunion belongs to a Hot Spot in the Indian Ocean and is comprised of Holocene, Quaternary and older volcanic rocks. The geological map was digitized from Nehlig et al. (2006). The watershed area considered for this study is derived from Louvat and Allègre (1997). The rocks are divided into Holocene, non-Holocene and two different types of Quaternary rocks (Qu1, Qu2).

Qu1 is described as being younger than 340 ka, which results in a theoretical Holocene fraction of 11.7 ka / 340 ka.

The age of Qu2 ranges from 5 ka to 65 ka, providing a time span of 60 ka. 6.7 ka lay within the Holocene time span (11.7 ka – 5 ka), so that the Holocene fraction can be calculated by the ratio of 6.7 ka / 60 ka.

Thus, the total Holocene fraction is calculated by:

$$Holocene\ fraction = \frac{\left(Area\ Holocene + \left(Area\ Qu1 * \left(\frac{11.7}{340}\right)\right) + \left(Area\ Qu2 * \left(\frac{6.7}{60}\right)\right)\right)}{Total\ area}$$

providing a value of 28.13%.

Table S10: *Classification of the basaltic rocks of La Réunion with the original data (first three columns) and our interpretation ("System/Series"). Note that "nn" represents that the age of the lithology is not known.*

ID	Definition	Type	System/Series
beta4	Coulées basaltiques	Massif du Piton de La Fournaise - Série du bouclier ancien (450,000 à 150,000 ans)	non-Holocene
tfp	Pitons et projections	Massif du Piton de La Fournaise	nn
beta7	Coulées basaltiques	Massif du Piton de La Fournaise - Série de la Plaine des Cafres (65,000 à 5,000 ans)	Quaternary2
beta6	Coulées basaltiques	Massif du Piton de La Fournaise - Série Plaine des Sables (65,000 à 5,000 ans)	Quaternary2
beta8	Coulées basaltiques	Massif du Piton de La Fournaise - Série volcanique subactuelle (<5,000 ans)	Holocene
beta5	Coulées basaltiques	Massif du Piton de La Fournaise - Série des Remparts (150,000 à 65,000 ans)	non-Holocene

beta3	Coulées différencciées	Massif du Piton de La Fournaise - Série alcaline anté-Fournaise (530,000 à 450,000 ans)	not considered
beta8e	Coulées basaltiques dans l'Enclos	Massif du Piton de La Fournaise - Série volcanique subactuelle (<5,000 ans)	Holocene
beta1	Coulées basaltiques à olivine	Massif du Piton des Neiges - Série des océanites (>340,000 ans)	non-Holocene
beta2	Coulées (basalte, hawaites, mugéarites)	Massif du Piton des Neiges - Série différenciée (<340,000 ans)	Quaternary1
Br	Brèches d'avalanches de débris de Saint Gilles	Massif du Piton des Neiges - Série différenciée (<340,000 ans)	Quaternary1
pc	Coulées ignimbritiques	Massif du Piton des Neiges - Série différenciée (<340,000 ans)	Quaternary1
Tau	Coulées trachytiques du plateau de Belouve	Massif du Piton des Neiges - Série différenciée (<340,000 ans)	not considered

Table S11: *Summary of calculated areas of La Réunion. Note that "tfp" is considered as of non-Holocene age. The Holocene fraction is calculated by the above-mentioned equation considering Holocene area, Qu1 area, Qu2 area and the total area.*

Area Holocene (km^2)	**Area non-Holocene (km^2)**	**Area Qu1 (km^2)**	**Area Qu2 (km^2)**	**Total Area (km^2)**	**Holocene (%)**
208.11	285.29	157.71	199.37	850.48	27.73

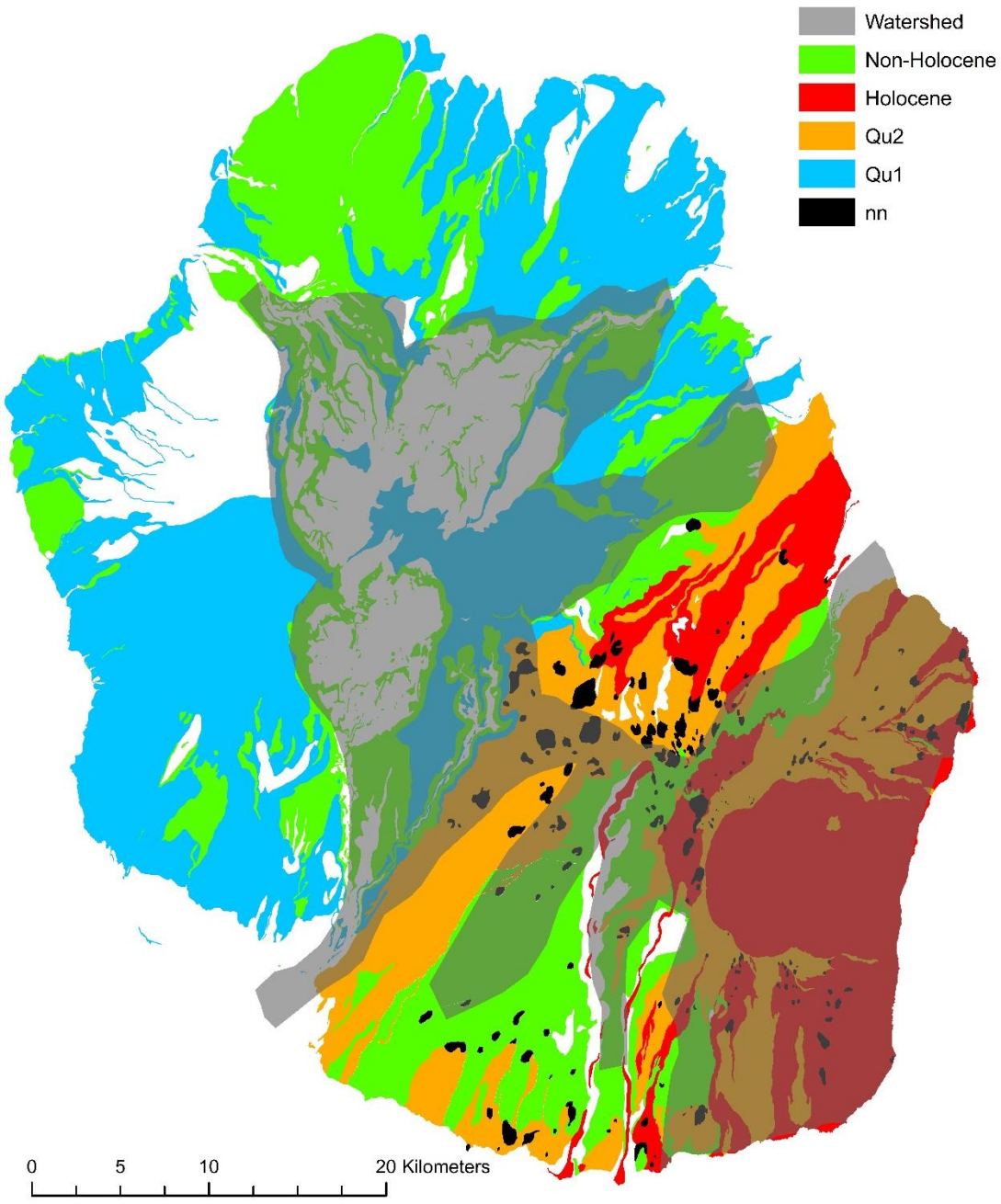

Figure S5: *Map of La Réunion showing the basaltic ages and additionally the watershed of the water samples. Only the watershed area was considered for this study.*

Wudalianchi Lake (No.25)

The basaltic rocks of Wudalianchi Lake are located in NE China and are of intraplate volcanic origin. The Geomap of Wudalianchi region was digitized after a map of the Ministry of Land and Resources of PRC, 2003 (unpublished work). The basalts are of Holocene and non-Holocene age. The Holocene fraction is 14.82%.

Table S12: *Classification of basalts of Wudalianchi Lake with the original map data (first three columns) and our interpretation shown in the column "System/Series".*

Symbol	Litho	Age	System/Series
betaQ2w	basalt	Middle Pleistocene	non-Holocene
betaQ1j	basalt	Lower Pleistocene	non-Holocene
betaQ2b	basalt	Middle Pleistocene	non-Holocene
betaQ1g	basalt	Tertiary	non-Holocene
betaQ42l	basalt	Holocene	Holocene

Table S13: *Calculated areas of Wudalianchi Lake. The Holocene fraction is calculated by Holocene area/Total area.*

Area Holocene (km^2)	Area non-Holocene (km^2)	Area Quaternary (km^2)	Total Area (km^2)	Holocene (%)
69.68	400.35	0	470.03	14.82

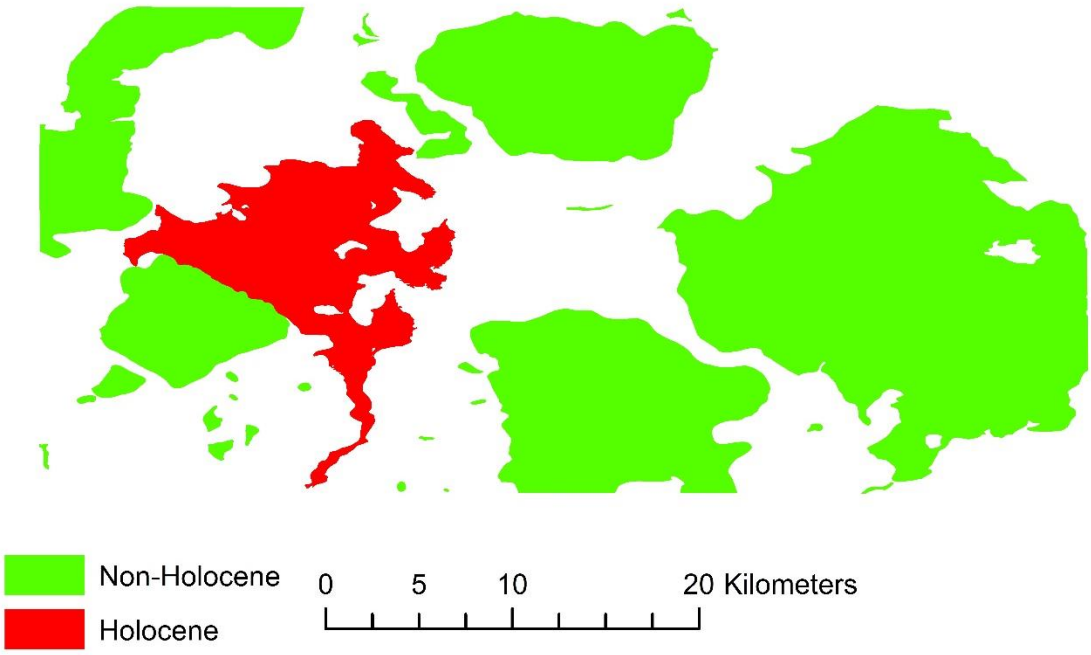

Figure S6: *Map of Wudalianchi Lake showing the distribution of Holocene and non-Holocene basaltic rocks.*

Japan (No.26)

The geological data was taken from the Global Lithological Map (GLiM) by Hartmann and Moosdorf (2012). Only watersheds of sample locations from the GLORICH database (Hartmann et al., 2014) were used. The basaltic rocks (attribute xx = 'vb' in the GLiM) are classified into Holocene, non-Holocene and Quaternary rocks. The calculation procedure of the Holocene fraction of Quaternary rocks is the same as for the Virunga Province (No.23), and a final Holocene percentage of 8.70% is calculated.

Table S14: *Classification of basaltic rocks for Japan after the GLiM (first three columns) and our interpretation "System/Series".*

xx	Age_Min	Age_Max	System/Series
vb	Holocene	Holocene	Holocene
vb	Neogene	Neogene	non-Holocene
vb	Paleogene	Paleogene	non-Holocene
vb	Paleozoic	Proterozoic	non-Holocene
vb	Pleistocene	Pleistocene	non-Holocene
vb	Pliocene	Pliocene	non-Holocene
vb	Quaternary	Quaternary	Quaternary

Table S15: *Calculated areas for the basaltic watersheds in Japan. Note that the Holocene fraction is calculated considering Holocene area, Quaternary area and total area.*

Area Holocene (km^2)	Area non-Holocene (km^2)	Area Quaternary (km^2)	Total Area (km^2)	Holocene (%)
243.30	2,216.41	354.44	2,814.15	8.70

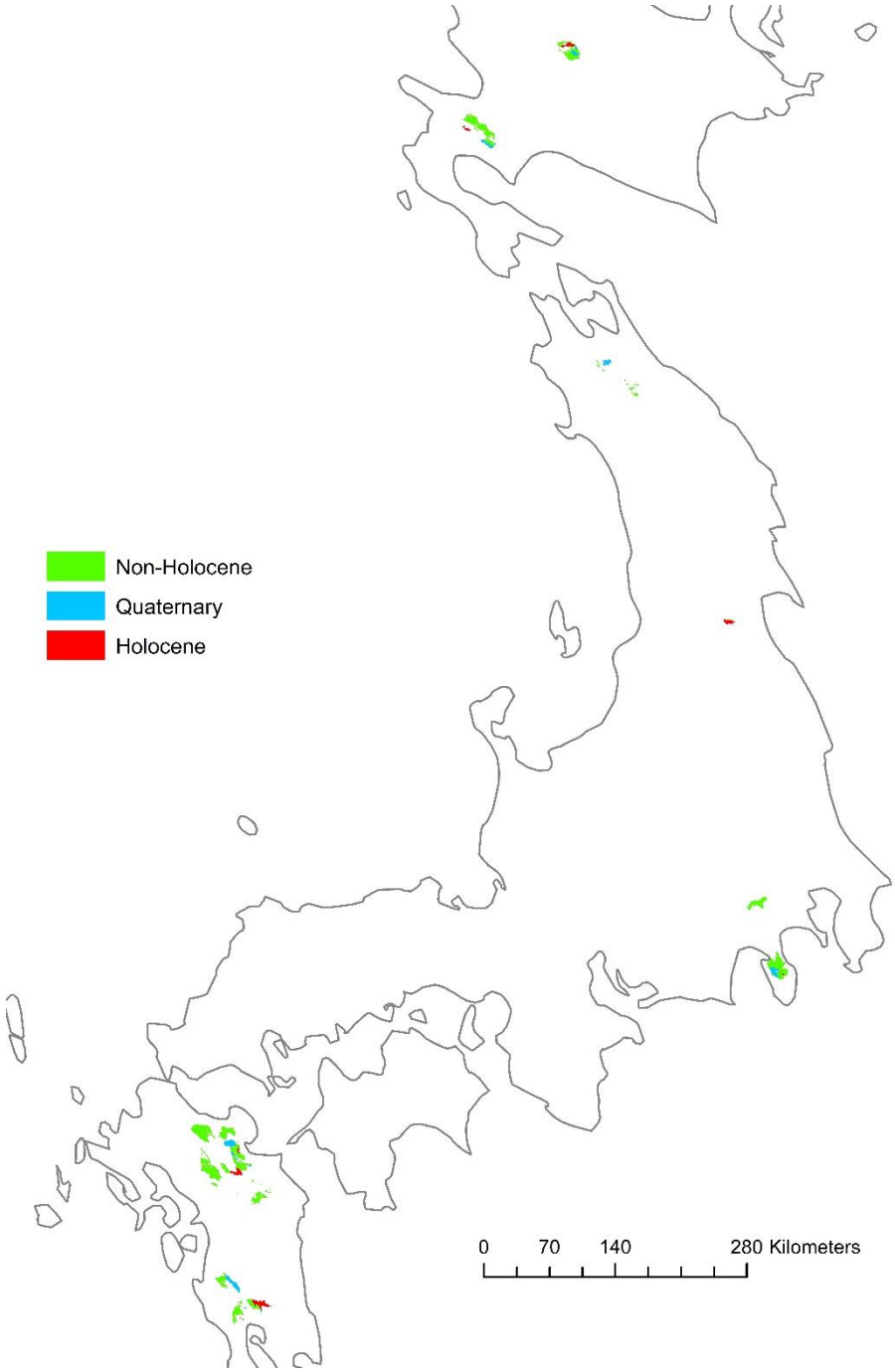

Figure S7: *Map showing the watersheds and age classification of basaltic rocks for Japan.*

Kamchatka (No.27)

The information of the basaltic rocks of the Kamchatka Peninsula is taken from the GLiM, attribute xx=’vb’ (Hartmann and Moosdorf, 2012) with the age classes Holocene, non-Holocene and Quaternary. The Holocene fraction was calculated as for the Virunga province (No.23). The watershed was calculated using sampling locations of Dessert et al. (2009). The Holocene fraction of the watershed of the Kamchatka Peninsula is 2.28%.

Table S16: *Classification of basaltic rocks of the Kamchatka Peninsula after the GLiM (first three columns) and our interpretation (“System/Series”).*

Rock_Description	Age_Min	Age_Max	System/Series
Basalte, Andesite und deren Tuffe	Lower Quaternary	Lower Quaternary	non-Holocene
Basalte, Andesite und deren Tuffe	Middle Quaternary	Middle Quaternary	non-Holocene
Volcanogenic formations, basic composition	Pliocene	Pliocene	non-Holocene
Basalte, Andesite und deren Tuffe	Quaternary	Quaternary	Quaternary
Volcanogenic formations, basic composition	Upper Cretaceous	Upper Cretaceous	non-Holocene
Basalte, Andesite und deren Tuffe	Upper Quaternary	Middle Quarernary	Quaternary
Basalte, Andesite und deren Tuffe	Upper Quaternary	Upper Quaternary	Holocene

Table S17: *Calculated areas of the Kamchatka Peninsula. Note that the Holocene fraction is calculated considering Holocene area, Quaternary area and total area.*

Area Holocene (km^2)	Area Non-Holocene (km^2)	Area Quaternary (km^2)	Total Area (km^2)	Holocene (%)
183.60	5,588.34	2,850.52	8,622.46	2.28

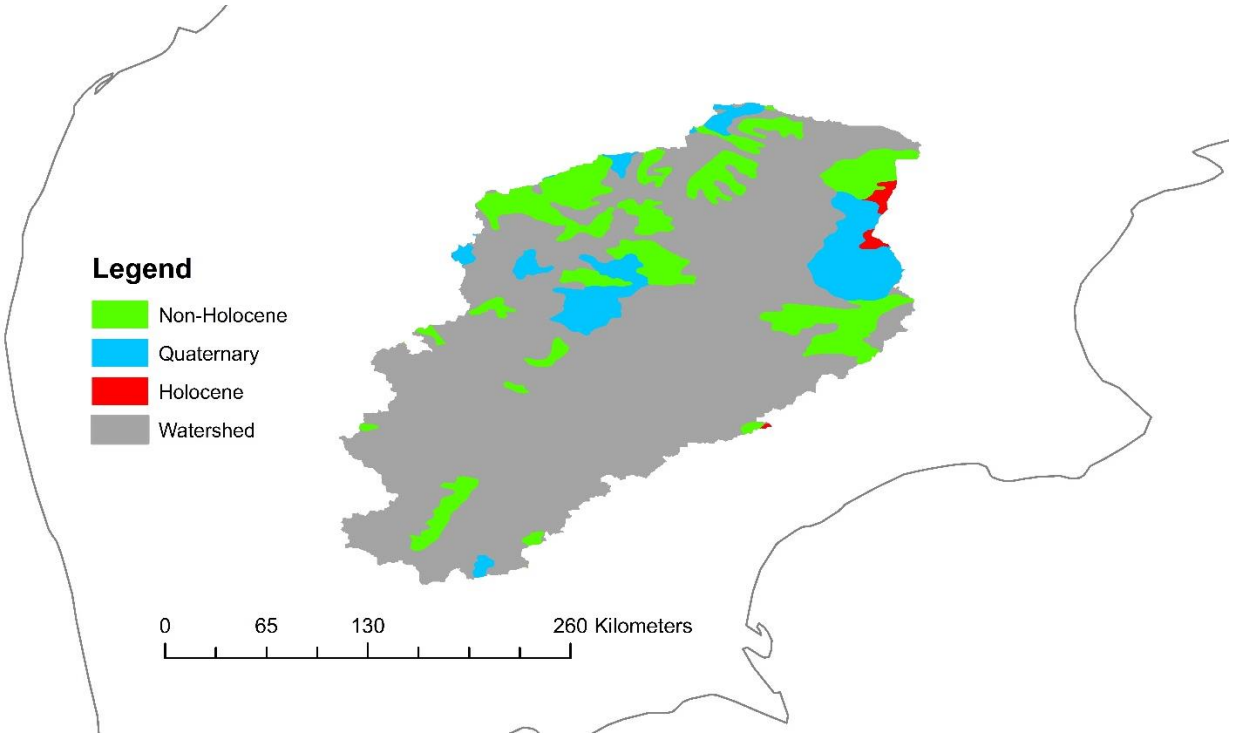

Figure S8: *Map showing the watershed of the Kamchatka Peninsula.*

Taranaki (No.28)

The Taranaki volcano is located in the southern part of the Northern Island of New Zealand. Price et al. (1992) define four different regions of the Taranaki Volcanics (Paritutu, Kaitake, Pouakai and Egmont), with Mt. Egmont as the youngest one. After Price et al. (1992) and references therein the cone of Mt. Egmont represents about 8% of the total eruptive mass and is of an age of about 10 ka (Holocene). Note that Mt. Egmont is not only composed of basalts but also of basaltic andesites and andesites (Price et al., 1992). We assume here a predominantly basaltic composition.

Big Island, Hawaii' (No.29)

The geological map of Big Island of Hawaii' was digitized after a map of Stearns and Macdonald (1946). The Holocene fraction of the Kilauea and Mauna Loa was calculated as:

$$Holocene\ fraction\ of\ Quaternary\ areas = Area\ Quaternary * (\frac{11{,}700}{126{,}000})$$

with the assumption that "Latest Pleistocene" = Upper Pleistocene (0.126Ma).

The total Holocene fraction is 14.08%, calculated by:

$$Holocene\ fraction = \frac{\left(Area\ Holocene + Area\ Quaternary * \left(\frac{11{,}700}{126{,}000}\right)\right)}{Total\ area}$$

Table S18: *Classification of the basaltic rocks of Big Island of Hawaii' after Stearns and Macdonald (1946) and our interpretation ("System/Series").*

Id	Volcano	Description	Age	System/Series
0	Kohala Mountain	Hawii' Volcanic Series, Andesite	Pleistocene	not considered
1	Kohala Mountain	Pololu Volcanic Series	Pliocene and older	non-Holocene
2	Mauna Kea Volcano	Recent lavas	Holocene	Holocene
3	Mauna Kea Volcano	Pleistocene lavas	Pleistocene	non-Holocene
4	Mauna Kea Volcano	Hamakua Volcanic Series, capped by Pahala ash	Pleistocene	non-Holocene
5	Hualalai Volcano	Historic lavas	Holocene	Holocene
6	Hualalai Volcano	Prehistoric lavas, partly younger or older than Waawaa volcanics	Quaternary	non-Holocene
7	Hualalai Volcano	Waawaa Volcanics (pumice cone, trachyte lava flow, partly covered with basaltic lavas and Pahala ash)	Pleistocene	not considered
8	Kilauea Volcano	Historic lavas	Holocene	Holocene
9	Kilauea Volcano	Prehistoric lavas	Recent and latest Pleistocene	Quaternary
10	Kilauea Volcano	Hilina Volcanic Series, capped by Pahala ash	Pleistocene	non-Holocene

11	Mauna Loa Volcano	Historic lavas	Holocene	Holocene
12	Mauna Loa Volcano	Prehistoric lavas	Recent and latest Pleistocene	Quaternary
13	Mauna Loa Volcano	Kahuku Volcanic Series, capped by Pahala ash	Pleistocene	non-Holocene
14	Mauna Loa Volcano	Ninole Volcanic Series	Pliocene or older	non-Holocene

Table S19: *Summary of the calculated areas for Big Island of Hawaii'. The Holocene fraction was calculated applying the above-mentioned equation considering the Holocene area, Quaternary area and total area.*

Area Holocene (km^2)	**Area Non-Holocene (km^2)**	**Area Quaternary (km^2)**	**Total Area (km^2)**	**Holocene (%)**
929.17	3,786.30	5,535.87	10,251.34	14.08

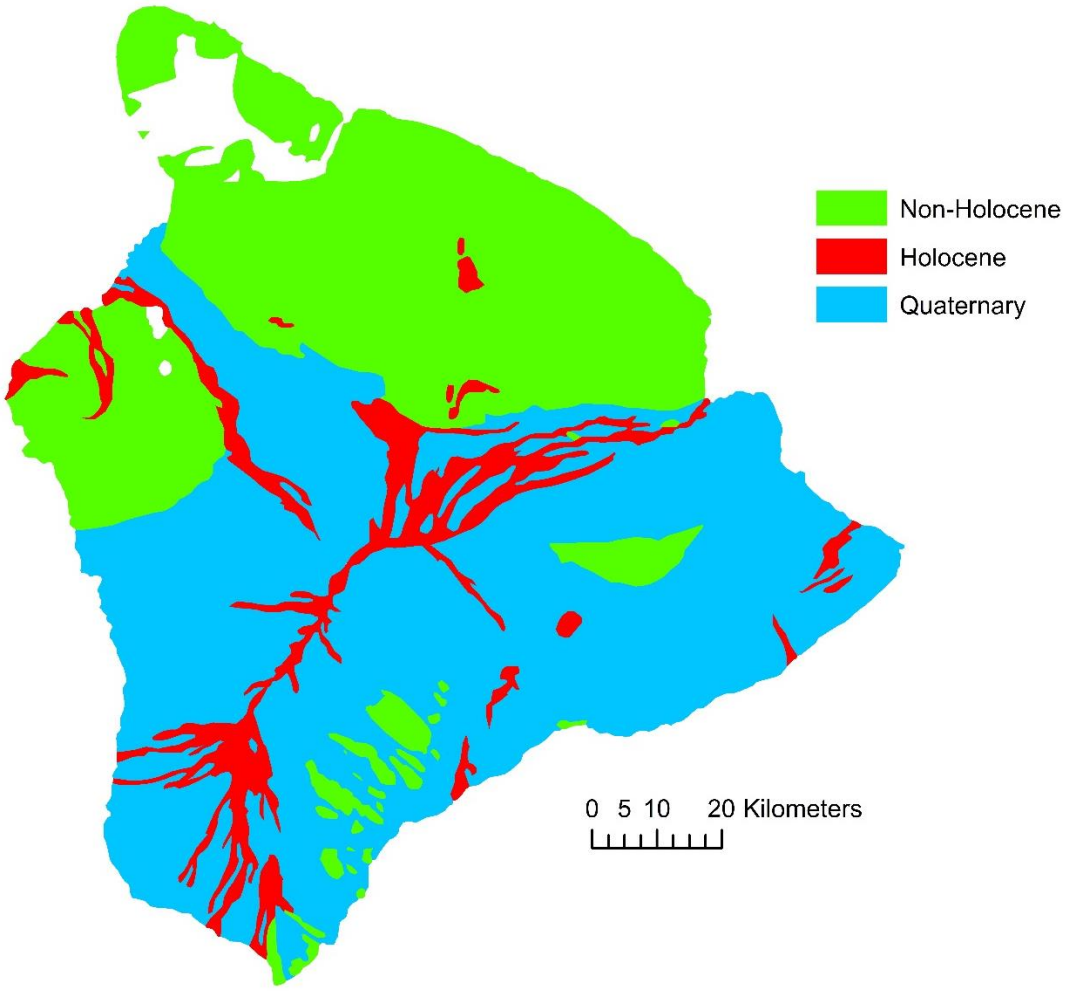

Figure S9: *Map of Big Island of Hawaii' showing the different age distributions of basaltic rocks.*

High Cascades (No.30)

The geological information for the High Cascades was taken from the GLiM by Hartmann and Moosdorf (2012). The Holocene fraction was calculated as for the Virunga province (No.23) and is 0.20%. The shapefiles of the watersheds are based on the GLORICH database (Hartmann et al., 2014).

Table S20: *Classification of the basaltic rocks of the High Cascades Region after the Global Lithological Map, attribute xx='vb' (first three columns) and our interpretation ("System/Series").*

Rock_Description	Age_Min	Age_Max	System/Series
Basalt;	Early to Middle Miocene	Early to Middle Miocene	non-Holocene
Tholeiite; siltstone	Eocene	Eocene	non-Holocene
Basalt; andesite	Late Eocene to Oligocene	Late Eocene to Oligocene	non-Holocene
Mafic volcanic rock;	Late Miocene to Pliocene	Late Miocene to Pliocene	non-Holocene
Basalt; volcanic breccia (agglomerate)	Middle Eocene to Late Eocene	Middle Eocene to Late Eocene	non-Holocene
Basalt (tholeiite); andesite	Middle Miocene	Middle Miocene	non-Holocene
Basalt;	Middle Miocene	Middle Miocene	non-Holocene
Andesite; basalt	Middle to Late Miocene	Middle to Late Miocene	non-Holocene
Basalt; andesite	Miocene	Miocene	non-Holocene
Basalt; rhyolite	Miocene-Pliocene	Miocene-Pliocene	non-Holocene
Basalt; volcanic breccia (agglomerate)	Oligocene to Miocene	Oligocene to Miocene	non-Holocene
Basalt; andesite	Pleistocene to Holocene	Pleistocene to Holocene	Quaternary
Basalt; andesite	Pliocene to Pleistocene	Pliocene to Pleistocene	non-Holocene
Andesite; basalt	Quaternary	Quaternary	Quaternary
Andesite; basalt	Tertiary (2-24 Ma)	Tertiary (2-24 Ma)	non-Holocene
Andesite; basalt	Miocene	Miocene	non-Holocene

Table S21: *Summarized area calculation for the watersheds of the High Cascades. The Holocene fraction was calculated as for the Virunga province (No. 23).*

Area Holocene (km^2)	Area Non-Holocene (km^2)	Area Quaternary (km^2)	Total Area (km^2)	Holocene (%)
0	3,033.92	2,479.39	5,513.31	0.20

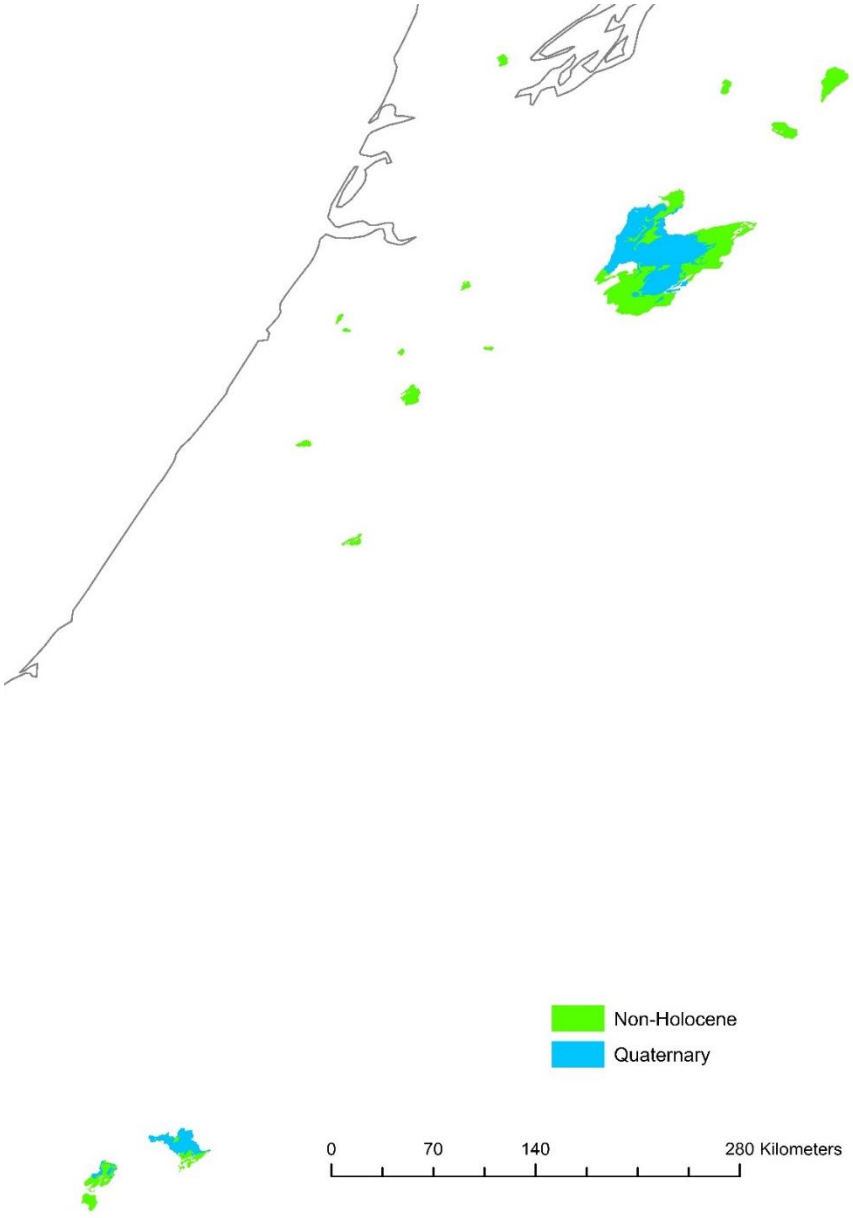

Figure S10: *Map of the watersheds of the High Cascades.*

Iceland (No.31)

The information of the basaltic rocks of Iceland are taken from the GLiM (Hartmann and Moosdorf, 2012) and are classified into Holocene, non-Holocene and Quaternary (for the calculation see Virunga Province, No. 23) and results in a Holocene coverage of 13.19%.

Table S22: *Description of the basaltic rocks of Iceland after the GLiM, attribute xx='vb' (first three columns) and our interpretation ("System/Series").*

Rock_Description	Age_Min	Age_Max	System/Series
Basalt and andesite	Holocene (postglacial time)	Holocene (postglacial time)	Holocene
Basic and intermediate hyaloclastites, lavas and associated sediments	Late Pleistocene	Late Pleistocene	non-Holocene
Basic and intermediate lavas and pyroclastic rocks (mainly hyaloclastite)	Late Pliocene, Early Pleistocene, 3.3 -	Late Pliocene, Early Pleistocene, 3.3 -	non-Holocene
Ocean-floor basalt; on land also intermediate volcanic rocks and sedimentary rocks	Miocene	Miocene	non-Holocene
Basic and intermediate volcanic rocks with intercalated sedimentary rocks	Miocene-Early Pliocene, older than 3.3 M	Miocene-Early Pliocene, older than 3.3 M	non-Holocene
Ocean-floor basalt	Pliocene	Pliocene	non-Holocene
Ocean-floor basalt	Quaternary	Quaternary	Quaternary

Table S23: *Summary of the area calculation for Iceland. Note that the Holocene fraction is calculated as for the Virunga province (No. 23).*

Area Holocene (km^2)	Area Non-Holocene (km^2)	Area Quaternary (km^2)	Total Area (km^2)	Holocene (%)
13,196.86	86,773.61	104.36	100,074.83	13.19

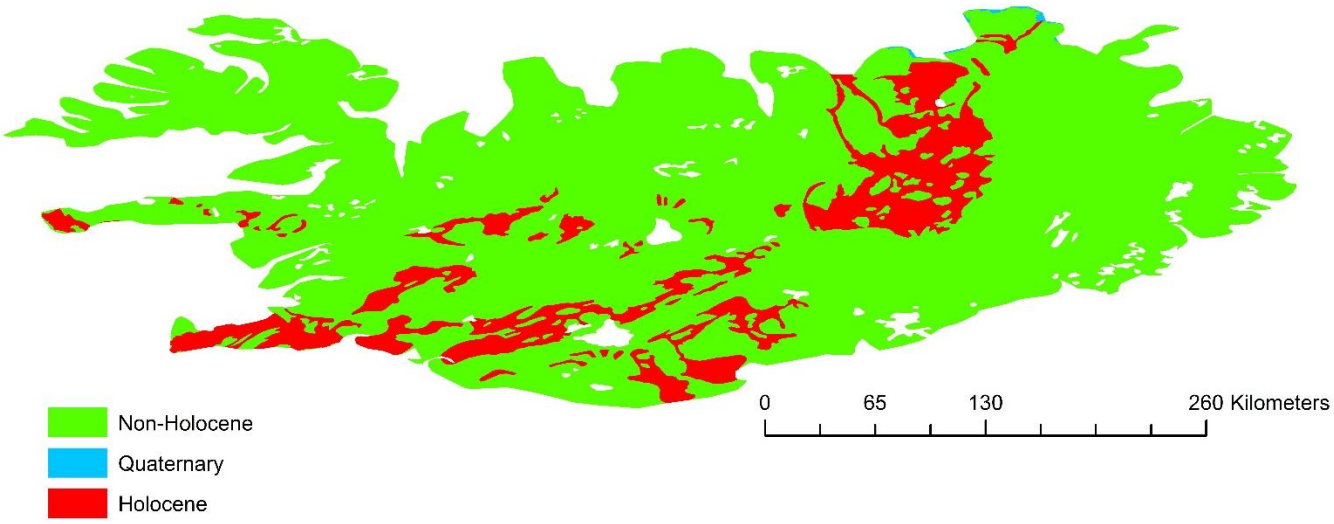

Figure S11: *Map of Iceland showing the distribution of the age of basaltic rocks.*

São Miguel Island (No.32)

São Miguel Island is related to a Hot Spot in the northern Atlantic. The geological map was digitized after Moore (1990). There are only two watersheds considered in this study (Freire et al., 2013). It was assumed that the Holocene area is proportional to the Holocene time span relative to the given mapped Quaternary age:

Qu1 (Agua de Pau Volcano, 0 – 200 ka):

$$Holocene\ fraction = Area\ Qu1 * (\frac{11{,}700}{200{,}000})$$

Qu2 (Furnas Volcano, 0 – 100 ka):

$$Holocene\ fraction = Area\ Qu2 * (\frac{11{,}700}{100{,}000})$$

The final Holocene fraction is 9.35% and is calculated by:

$$Holocene\ fraction = \frac{Area\ Qu1 * \left(\frac{11{,}700}{200{,}000}\right) + Area\ Qu2 * \left(\frac{11{,}700}{100{,}000}\right)}{Total\ Area}$$

The watershed areas are of trachytic composition, therefore São Miguel was excluded from the calculations (eq. 5 in the main text) but were kept for comparison because of the generally basaltic environment of the island.

Table S24: *Classification of the rocks of the watersheds of São Miguel from the original data and our interpretation ("System/Series").*

Id	Name	Type	Age	System/Series
2	Agua de Pau Volcano	Trachyte stratovolcano	0-200ka	Qu1
4	Furnas Volcano	Trachyte stratovolcano	0-100ka	Qu2

Table S25: *Summary of the calculated areas of the watersheds of São Miguel. The Holocene fraction was calculated by the above-mentioned equation.*

Area Holocene (km^2)	Area Non-Holocene (km^2)	Area Qu1 (km^2)	Area Qu2 (km^2)	Total Area (km^2)	Holocene (%)
0	0	18.86	28.18	47.04	9.35

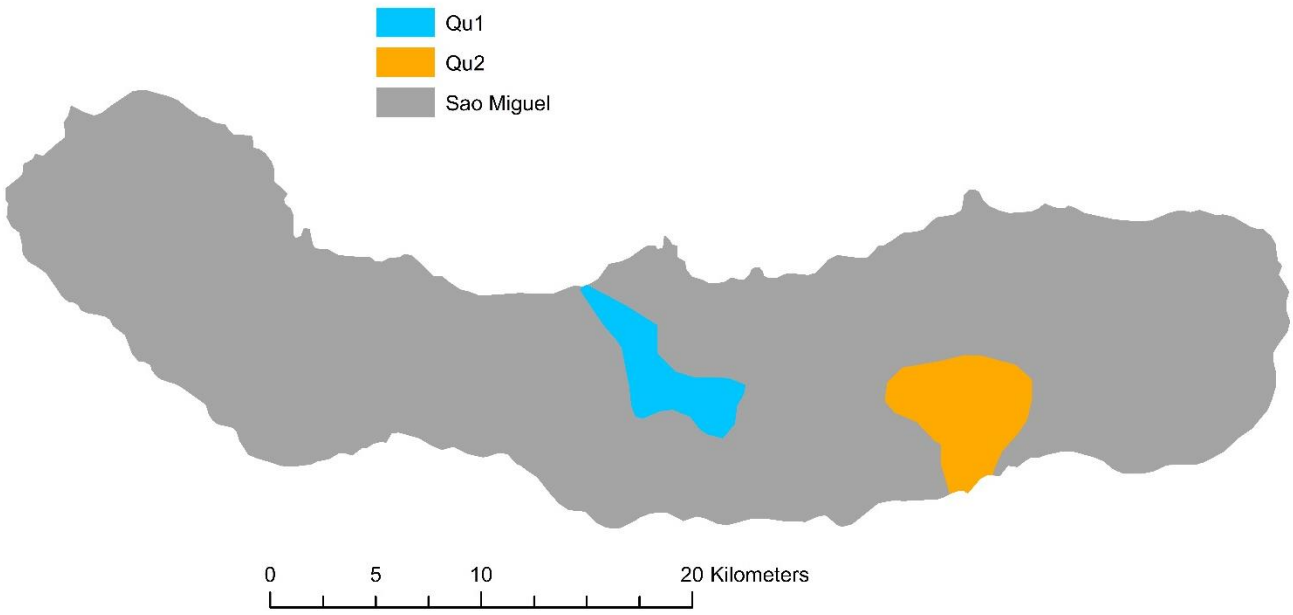

Figure S12: *Map of São Miguel showing the two watersheds considered in this study.*

Tianchi Lake (No.33)

The geological map of the Tianchi Lake region was digitized after Paone and Yun (2016). The rocks are directly separated into Holocene and non-Holocene age. The total catchment area is 11.31 km² and the Holocene fraction area is 65.34%. The value for the runoff was calculated after Fekete et al. (2002).

Table S26: *Description of the rocks of Tianchi Lake after Paone and Yun (2016) (first column) and our interpretation ("System/Series").*

Description	System/Series
Second fan-shaped debris flow - Holocene	Holocene
Rock-fall deposit - Holocene?	Holocene
1668 dark trachytic ignimbrite and surge - Holocene	Holocene
Third fan-shaped debris flow - Holocene	Holocene
1903 phreatomagmatic eruption - Holocene	Holocene
Baitoushan III upper trachyte cone with comendite, 0.02-0.22 Ma	non-Holocene
Baithoushan II middly trachyte cone and ignimbrite, 0.25-0.44 Ma	non-Holocene

Since the lithology is mostly described as trachytic, Tianchi Lake was excluded from the calculations (eq. 5, main text) but kept in this study for comparison.

Table S27: *Summary of the area calculation for Tianchi Lake. The Holocene fraction was calculated by the ratio of Holocene area/Total area.*

Area Holocene (km^2)	Area non-Holocene (km^2)	Area Quaternary (km^2)	Total Area (km^2)	Holocene (%)
7.39	3.92	0	11.31	65.34

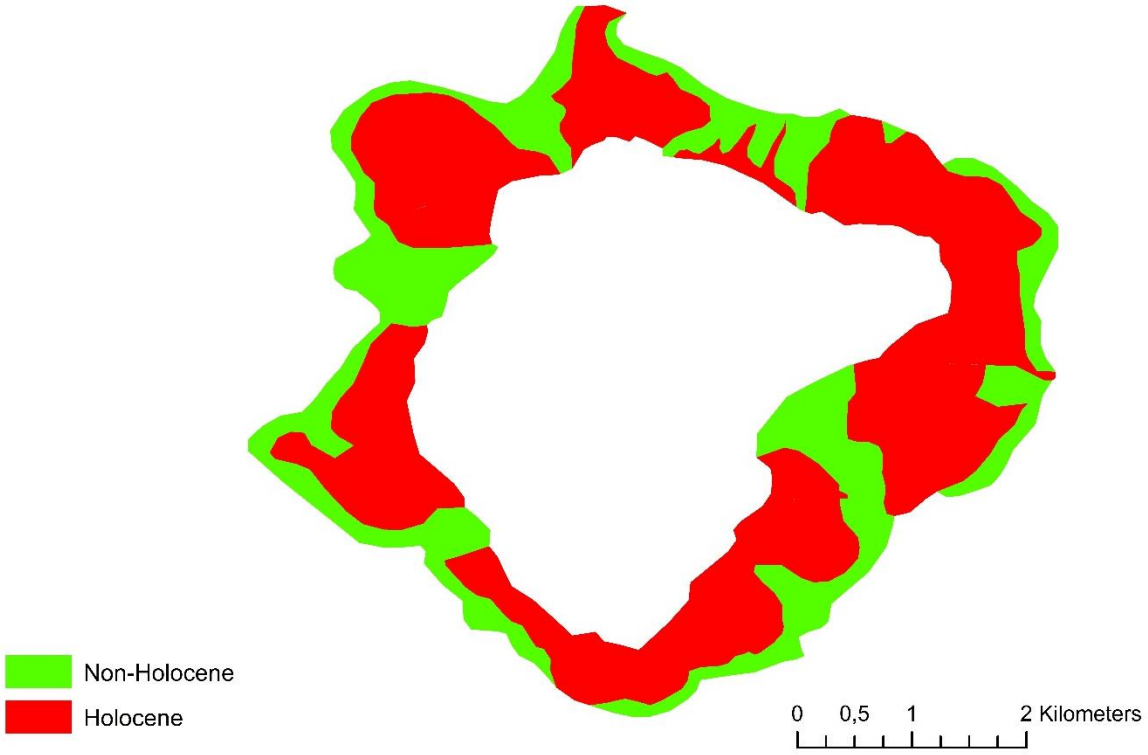

Figure S13: *Map of Tianchi Lake and its surrounding lithology showing the distribution of the age of rocks.*

Supplemental Material C: Saturation state with respect to calcite

Data used in the previous study of Li et al. (2016) was derived by published literature and the GLORICH database (Hartmann et al., 2014), but also new river sites of China are included (for more details see Supplementary information of Li et al. (2016). Li et al. (2016) used either alkalinity or DIC concentrations to calculate the alkalinity flux rates of the individual basaltic volcanic areas. They calculated the alkalinity flux rates by multiplying the mean concentration of dissolved inorganic carbon (DIC) by the annual runoff.

For six areas full water chemistry data are available (High Cascades, Japan, Northeast America, Southeast Australia, South Africa and Tasmania), while for others either pH or major cations were not available. For these available data (103 catchments) the saturation index for calcite was calculated. In general, water samples are undersaturated with respect to calcite (77%). From the oversaturated samples 50% have values close to 0 with a saturation index SI < 0.5. A SI ~ 0.5 is the typical value for rivers in limestone areas (Romero-Mujalli et al., 2018). The other 12 values are between SI = 0.5 and 0.9 and according water sample locations are mostly in dry areas of South Africa or Australia.

In general, younger active areas have significant contributions of magmatic SO_4 or Cl, which shifts the saturation states normally further to lower, negative values. We cannot conclude from the river data what happens in the aquifer system but reference the study of Jacobson et al. (2015) in the main text. They quantified the contribution of trace calcite dissolution from basalt using Ca-isotope data.

Supplemental Material D: Additional relations between Alkalinity, Reactivity and Holocene area fraction

In addition to results provided in the main text further relationships among applied parameters are shown.

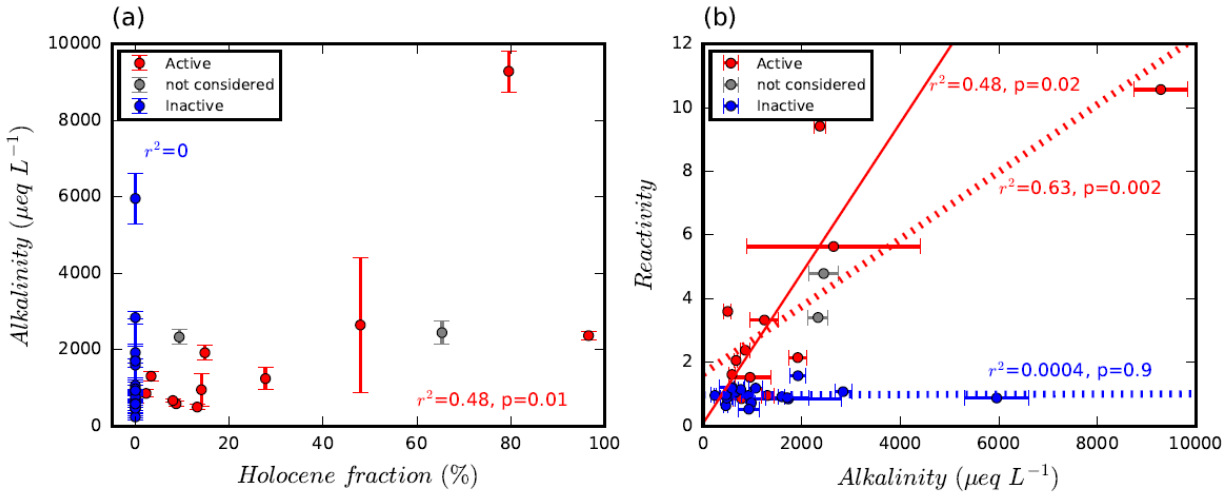

Figure S14: *Scatterplot relationships between alkalinity, Holocene fraction and Reactivity. a) Holocene fraction versus alkalinity concentrations (blue: IVFs, red: AVFs). b) Alkalinity concentration versus Reactivity: For the AVFs the coefficient of determination is r^2=0.63 (p=0.002). However, if removing the one "outlier" with elevated alkalinity concentration (Mt. Etna), it is not concluded that elevated alkalinity concentrations are responsible in general for observed elevated Reactivity of AVFs, considering the alkalinity concentration distribution for IVF. However, a relevant correlation exists between alkalinity and Reactivity for AVFs. The solid red regression line shows the correlation of AVFs excluding Mt. Etna (r^2=0.48, p=0.02).*

Supplemental Material E: Estimation of the parameters for the new scaling law

The new scaling law for alkalinity fluxes (eq. 5, main text) was derived by a Monte Carlo method. Temperature and alkalinity flux rates were selected randomly 10,000 times within the range of ± one standard deviation for each volcanic field:

$$X = \bar{x} + std * (2 * rand - 1)$$

With X = calculated random value for temperature or alkalinity flux rate,

$\overline{x}$ = mean value of temperature or alkalinity flux rate,

std = standard deviation of temperature or alkalinity flux rate

"Rand" is a function from Matlab software, which creates uniformly distributed random numbers between 0 and 1 (The MathWorks Inc.: MATLAB R2016a).

The calculated standard deviations of weighted mean values σ_m for temperature and alkalinity flux rates (Table S1) are taken from Li et al. (2016). The new scaling law is represented by the equation:

$$Alkalinity\ flux\ rate = (1 + b1 * Holocene\ fraction) * b2 * e^{b3 * Temperature}$$

Applying the Levenberg-Marquardt algorithm to the 10,000 sets of alkalinity flux rates and temperature the following mean b-parameters of the equation were found:

b_1 = 0.10 with standard deviation=0.02 and median = 0.10

b_2 = 0.23 with standard deviation=0.09 and median = 0.23

b_3 = 0.06 with standard deviation=0.02 and median = 0.06

The root mean square error (RMSE) of eq. 5 in the main text is 0.3, calculated by the following equation:

$$RMSE = \sqrt{\frac{\sum(residual)^2}{n-2}}$$

Calculating the regression of calculated alkalinity flux rates and estimated alkalinity flux rates by the new scaling law provides an r^2=0.96 and $p<10^{-3}$.

The linear regression of Holocene fractions and Reactivity for AVFs gives an r^2=0.93 and p=0.01.

Supplemental Material F: Global calculations CO_2 consumption by basalt weathering

The global CO_2 consumption fluxes (table S28 and S29, and table 1 in the main text) were calculated 10,000 times for each grid cell using the produced set of b-parameters (Levenberg-Marquardt-algorithm see above, Supplemental Material E), global temperature and runoff information (Fekete et al., 2002; Hijmans et al., 2005), as well as the new global basalt map (Fig. S15). Finally, we calculated the mean values of the set of global CO_2 consumption rates, the standard deviations and the percentiles for 25% and 75% of the global fluxes. The standard deviations and percentiles represent the dispersion of random correlations and not the uncertainty given by the residuals.

The global basalt map, mostly based on the GLiM (Fig. S15) distinguishes Holocene, Cenozoic and non-Cenozoic basaltic areas. The calculations were conducted with a 20 km grid resolution.

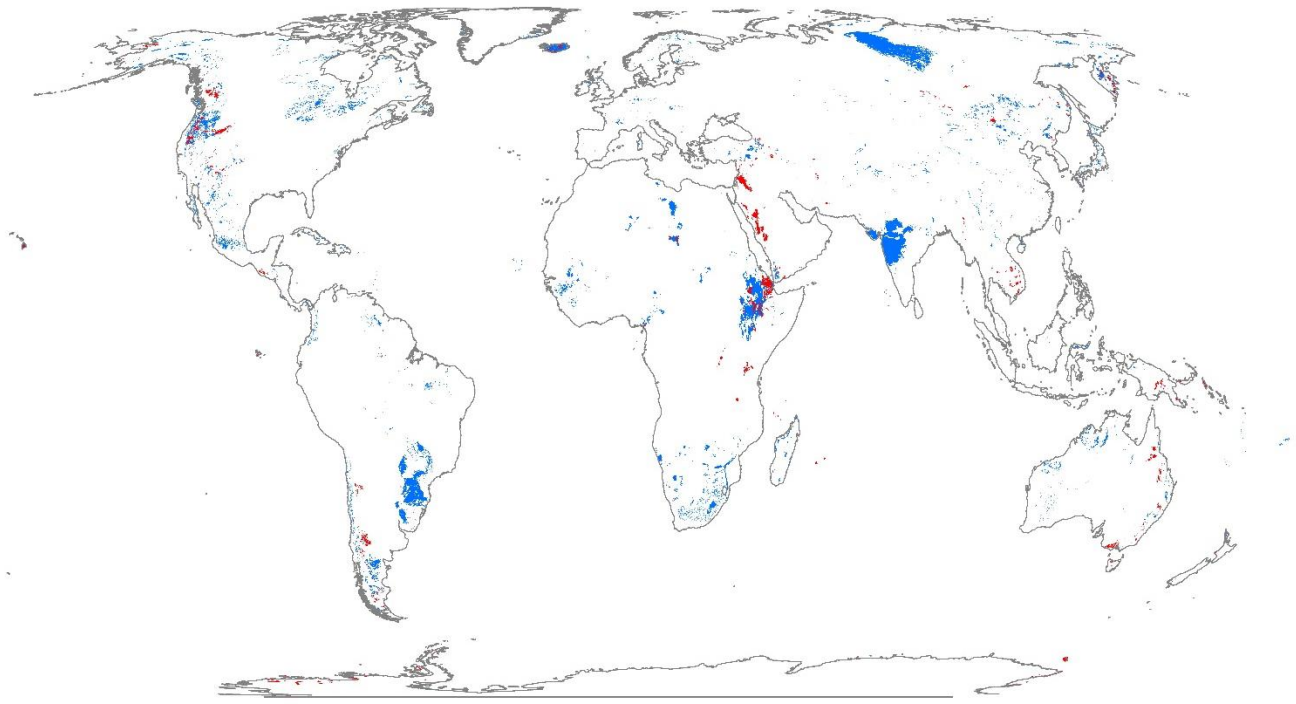

Figure S15: *Global distribution of basalt areas distinguishing Cenozoic (red) and Non-Cenozoic areas (blue). The reported Holocene fractions of the Cenozoic areas are considered in the global calculation. Some areas with missing age information were*

considered as of non-Holocene age and may result in a smaller global Holocene area fraction applied for global calculations. The map is described in Supplemental Material G.

For comparison the global CO_2 consumption was calculated only once by applying the new scaling law with the mean of the set of three b-parameters to every grid cell, and using the global datasets of temperature and runoff (Fekete et al., 2002; Hijmans et al., 2005), as well as the global basalt map. Here, the global flux with runoff restriction is 2×10^{12} mol a^{-1}.

Adding the root mean square error of the 10,000 global calculations of the CO_2 consumption from above to every grid cell results in a flux of 3×10^{12} mol a^{-1} and substracting the root mean square error to every grid cell results in 1×10^{12} mol a^{-1}, which is representing the range of uncertainty. This range of uncertainty might be overestimating the uncertainty for low CO_2 consumption values and underestimating the uncertainty for high CO_2 consumption values, since the residuals are not normally distributed.

Table S28: *Global calculations of CO_2 consumption for areas with a runoff >74mm/a. As reference previous global empirical equations (Bluth and Kump, 1994; Amiotte-Suchet and Probst, 1995; Dessert et al., 2003; Goll et al., 2014, without soil shielding to mimic the relevance of temperature) were applied to derive global CO_2 consumption values. The values of the new scaling law in this table and in table S29 are given by simulating 10,000 runs (see above). "p25" and "p75" represent the calculated percentiles of 25% and 75%, respectively and "std" the standard deviation.*

	Total Area [km^2]	Holocene Area [km^2]	% of global basalt area	CO_2 consumption [10^6 mol/a]								Area [km^2] for q>74mm/a	Holocene area [km^2] for q>74mm/a
				Goll et al., 2014	Dessert et al., 2003	Amiotte-Suchet & Probst, 1995	Bluth & Kump, 1994	New scaling law	p25	p75	std		
Fluxes from purely Holocene areas	48,593	48,593	0.92	15,531	17,453	13,560	10,060	100,037	89,216	109,234	14,487	29,213	29,213
Raster with Holocene influence (Cenozoic)	903,600	48,593	17.03	225,938	239,122	112,221	88,208	283,726	276,351	292,969	13,074	338,800	29,213
Raster without Holocene influence (Non-Cenozoic)	4,401,200	-	82.97	1,340,243	1,430,216	750,618	658,218	1,646,033	1,586,658	1,708,683	91,215	3,059,600	-
TOTAL	5,304,800	48,593	100.00	1,566,181	1,669,338	862,839	746,427	1,929,759	1,868,357	1,992,574	92,519	3,398,400	29,213

Table S29: *Global CO_2 consumption by basalt weathering without runoff restriction as applied in Table S28.*

	Total Area [km^2]	Holocene Area [km^2]	% of global basalt area	CO_2 consumption [10^6 mol/a]							
				Goll et al., 2014	Dessert et al., 2003	Amiotte-Suchet & Probst, 1995	Bluth & Kump, 1994	New scaling law	p25	p75	std
Fluxes from purely Holocene areas	48,593	48,593	0.92	15,646	17,577	13,628	10,209	209,602	195,275	223,222	19,264
Raster with Holocene influence (Cenozoic)	903,600	48,593	17.03	227,716	241,036	113,265	90,347	735,004	707,519	763,323	38,618
Raster without Holocene influence (Non-Cenozoic)	4,401,200	-	82.97	1,351,814	1,442,505	756,928	670,733	2,534,801	2,434,265	2,646,095	161,340
TOTAL	5,304,800	48,593	100.00	1,579,530	1,683,541	870,193	761,081	3,269,805	3,150,147	3,404,366	193,745

Supplemental Material G: Enhanced global basalt map beyond GLiM

A new global basalt map was created combining several datasets. Main input is the Global Lithological Map (GLiM) (Hartmann and Moosdorf, 2012). New, additional data were taken from geological maps that were considered for the development of the Global Unconsolidated Sediments Map database(GUM) (Börker et al., 2018) and the individual active volcanoes described in this study. For the individual calculation of Holocene percentages see following tables.

Table S30: *Table showing the ages of the basaltic fields of the GLiM with the authors interpretation (third column). Note that only areas with Holocene fraction are listed. All other age descriptions of the GLiM were considered as of non-Holocene age.*

Age_Min	Age_Max	HoloceneArea
Cainozoic	Cainozoic	0.02
Cenozoic	Cenozoic	0.02
Oligocene	Cainozoic	0.02
Quaternary	Tertiary	0.02
Quaternary	Cainozoic	0.02
Quaternary and Tertiary	Quaternary and Tertiary	0.02
QUATERNARY OR TERTIARY	QUATERNARY OR TERTIARY	0.02
Tertiary(?) and Quaternary	Tertiary(?) and Quaternary	0.02
Tertiary-Quaternary	Tertiary-Quaternary	0.02
Oligocene and younger	Oligocene and younger	0.03
Holocene	Miocene	0.05
Miocene to Holocene	Miocene to Holocene	0.05
Miocene to Quaternary	Miocene to Quaternary	0.05
Neogene	Quaternary	0.05
Neogene to Holocene	Neogene to Holocene	0.05
Quaternary	Neogene	0.05
PLIOCENO-PLEISTOCENO-HOLOCENO	PLIOCENO-PLEISTOCENO-HOLOCENO	0.22
Quaternary	Pliocene	0.22
Quaternary to Pliocene	Quaternary to Pliocene	0.22
Quaternary (0-4 Ma)	Quaternary (0-4 Ma)	0.29
Middle Pliocene to Holocene	Middle Pliocene to Holocene	0.33
Holocene	Pleistocene	0.45
Pleistocene to Holocene	Pleistocene to Holocene	0.45
Quaternary	Upper Quaternary	0.45
Quaternary	Pleistocene	0.45
Quaternary	Quaternary	0.45
Upper Quaternary	Middle Quarernary	0.45
Late Pleistocene to Holocene	Late Pleistocene to Holocene	9.29
Holocene	Holocene	100
Holocene (postglacial time)	Holocene (postglacial time)	100
Upper Quaternary	Upper Quaternary	100

Table S31: *Table showing the age classifications of additional data of several geological maps that were used for the GUM database with our interpretation (third column). Only the quaternary lithologies were considered. Map sources are: Afghanistan (Doebrich et al., 2006), Australia (Raymond et al., 2012), Austria (Geologische Bundesanstalt (GBA), 2013), Canada (Fulton, 1995), China (China Geological Survey, 2002), Colombia (Gomez Tapias et al., 2015), Ethiopia (Tefera et al., 1996), Japan (Geological Survey of Japan AIST (ed.), 2009), Germany (Bundesanstalt für Geowissenschaften und Rohstoffe, 2007), Tanzania (Geological Survey of Tanzania, Geo-Economic Data (1:2M) - Geology, http://www.gmis-tanzania.com/, accessed May 2016), USA (Soller et al., 2009).*

Age_Min	Age_Max	HoloceneArea
1 M	0.26 M	0
2.5 M	0.26 M	0
0.215 M	0.19 M	0
Sarmatian/Pannonian	Plio/Pleistocene	0
Pliocene	Pleistocene	0
2.5 M	0.01 M	0
Early Pleistocene	Early Pleistocene	0
0.780	0.126	0
Middle Pleistocene	Middle Pleistocene	0
Late Pleistocene	Late Pleistocene	0
Pleistocene	Pleistocene	0
Middle Pleistocene	Late Pleistocene	0
Early Pleistocene	Middle Pleistocene	0
Cenozoic	Cenozoic	0.02
23 Ma	0 Ma	0.05
Pliocene	Holocene	0.22
Quaternary	Quaternary	0.45
Late Pleistocene	Holocene	9.29
Holocene	Holocene	100

References

Amiotte-Suchet, P., and Probst, J. L.: A global model for present-day atmospheric/soil CO2 consumption by chemical erosion of continental rocks (GEM-CO2), Tellus B, 47, 273-280, 10.1034/j.1600-0889.47.issue1.23.x, 1995.

Antun, P., Gerards, J., and Petricec, V.: Carte Géologique du Rwanda, Feuille Ruhengeri Nord (S2/29 NW et NE), Champs Volcanique des Birunga, Institut Géographique Militaire de Belgique, 1971.

Ateba, B., Dorbath, C., Dorbath, L., Ntepe, N., Frogneux, M., Aka, F. T., Hell, J. V., Delmond, J. C., and Manguelle, D.: Eruptive and earthquake activities related to the 2000 eruption of Mount Cameroon volcano (West Africa), Journal of Volcanology and Geothermal Research, 179, 206-216, 10.1016/j.jvolgeores.2008.11.021, 2009.

Balagizi, C. M., Darchambeau, F., Bouillon, S., Yalire, M. M., Lambert, T., and Borges, A. V.: River geochemistry, chemical weathering, and atmospheric CO2 consumption rates in the Virunga Volcanic Province (East Africa), Geochemistry, Geophysics, Geosystems, 16, 2637-2660, 10.1002/2015GC005999, 2015.

Benedetti, M. F., Dia, A., Riotte, J., Chabaux, F., Gérard, M., Boulegue, J., Fritz, B., Chauvel, C., Bulourde, M., and Déruelle, B.: Chemical weathering of basaltic lava flows undergoing extreme climatic conditions: the water geochemistry record, Chemical Geology, 201, 1-17, 2003.

Bluth, G. J., and Kump, L. R.: Lithologic and climatologic controls of river chemistry, Geochimica et Cosmochimica Acta, 58, 2341-2359, 1994.

Börker, J., Hartmann, J., Amann, T., and Romero-Mujalli, G.: Terrestrial sediments of the earth: development of a global unconsolidated sediments map database (GUM), Geochemistry, Geophysics, Geosystems, 19, 997-1024, 2018.

Branca, S., Coltelli, M., Groppelli, G., and Lentini, F.: Carta Geologica del vulcano Etna (Scala 1:50.000), Istituto Nazionale di Geofisica e Vulcanologia Osservatorio Etneo sezione di Catania, Istituto per la Protezione e la Ricerca Ambientale (ISPRA), Servizio Geologico d'Italia, CNR-Consiglio Nazionale delle Ricerche, Univerità di Catania Dipartimento di Scienze Geologiche, 2011a.

Branca, S., Coltelli, M., Groppelli, G., and Lentini, F.: Geological map of Etna volcano, 1: 50,000 scale, Italian Journal of Geosciences, 130, 265-291, 2011b.

Bundesanstalt für Geowissenschaften und Rohstoffe: Geologische Übersichtskarte der Bundesrepublik Deutschland (scale 1:200,000 (GÜK200)), Bundesanstalt für Geowissenschaften und Rohstoffe, Hannover, Germany, 2007.

China Geological Survey: Geological Atlas of China - Chinese geological map (scale 1:2,500,000), Geological Press, Beijing, 2002.

De Mulder, M., Hertogen, J., Deutsch, S., and André, L.: The role of crustal contamination in the potassic suite of the Karisimbi volcano (Virunga, African Rift Valley), Chemical geology, 57, 117-136, 1986.

Dessert, C., Dupré, B., Gaillardet, J., François, L. M., and Allègre, C. J.: Basalt weathering laws and the impact of basalt weathering on the global carbon cycle, Chemical Geology, 202, 257-273, http://dx.doi.org/10.1016/j.chemgeo.2002.10.001, 2003.

Dessert, C., Gaillardet, J., Dupre, B., Schott, J., and Pokrovsky, O. S.: Fluxes of high- versus low-temperature water–rock interactions in aerial volcanic areas: Example from the Kamchatka Peninsula, Russia, Geochimica et Cosmochimica Acta, 73, 148-169, 10.1016/j.gca.2008.09.012, 2009.

Doebrich, J. L., Wahl, R. R., Ludington, S. D., Chirico, P. G., Wandrey, C. J., Bohannon, R. G., Orris, G. J., and Bliss, J.: Geologic age and lithology of Afghanistan (glgafg.shp) (U.S. Geological Survey Open File Report: Issue Identification number 2006-1038), U.S. Geological Survey, Denver, CO. U.S.A., 2006.

Fekete, B. M., Vörösmarty, C. J., and Grabs, W.: High-resolution fields of global runoff combining observed river discharge and simulated water balances, Global Biogeochemical Cycles, 16, 15-01-15-10, 10.1029/1999gb001254, 2002.

Freire, P., Andrade, C., Coutinho, R., and Cruz, J. V.: Fluvial geochemistry in Sao Miguel Island (Azores, Portugal): source and fluxes of inorganic solutes in an active volcanic environment, Science of the Total Environment, 454-455, 154-169, 10.1016/j.scitotenv.2013.02.090, 2013.

Fulton, R.: Surficial materials of Canada. In Geological Survey of Canada (Editor), Map 1880A, scale 1:5 000 000, Natural Resources Canada, Ottawa, Canada, 1995.

Geological Survey of Japan AIST (ed.): Seamless digital geological map of Japan 1:200,000. Dec 15, 2009 version. Research Information Database DB084, https://gbank.gsj.jp/seamless/download/downloadIndex_e.html, accessed May 2016, Geological Survey of Japan, National Institute of Advanced Industrial Science and Technology, Japan, 2009.

Geological Survey of Tanzania: Geo-Economic Data (1:2M) - Geology, http://www.gmis-tanzania.com/, accessed May 2016

Geologische Bundesanstalt (GBA): Kartographisches Modell 1:500000 Austria - Geologie, Wien, Austria, 2013.

Gioncada, A., Gonzalez-Ferran, O., Lezzerini, M., Mazzuoli, R., Bisson, M., and Rapu, S. A.: The volcanic rocks of Easter Island (Chile) and their use for the Moai sculptures, European Journal of Mineralogy, 22, 855-867, 2010.

Goll, D. S., Moosdorf, N., Hartmann, J., and Brovkin, V.: Climate-driven changes in chemical weathering and associated phosphorus release since 1850: Implications for the land carbon balance, Geophysical Research Letters, 41, 3553-3558, 10.1002/2014GL059471, 2014.

Gomez Tapias, J., Nivia Guevara, A., Montes Ramirez, N. E., Diederix, H., Almanza Melendez, M. F., Alcarcel Gutierrez, F. A., and Madrid Montoya, C. A.: Explanatory notes: Geological Map of Colombia, in: Compilando la geologia de Colombia: Una vision a 2015. Servicio Geologico Colombiano, Publicaciones Geológicas Especiales 33, edited by: Gomez, J., and Almanza, M. F., Bogotá, 35-60, 2015.

Hartmann, J., and Moosdorf, N.: The new global lithological map database GLiM: A representation of rock properties at the Earth surface, Geochemistry, Geophysics, Geosystems, 13, Q12004, 10.1029/2012GC004370, 2012.

Hartmann, J., Lauerwald, R., and Moosdorf, N.: A brief overview of the GLObal RIver CHemistry Database, GLORICH, Procedia Earth and Planetary Science, 10, 23-27, 2014.

Hijmans, R. J., Cameron, S. E., Parra, J. L., Jones, P. G., and Jarvis, A.: Very high resolution interpolated climate surfaces for global land areas, International journal of climatology, 25, 1965-1978, 2005.

Jacobson, A. D., Grace Andrews, M., Lehn, G. O., and Holmden, C.: Silicate versus carbonate weathering in Iceland: New insights from Ca isotopes, Earth and Planetary Science Letters, 416, 132-142, http://dx.doi.org/10.1016/j.epsl.2015.01.030, 2015.

Le Maréchal, A.: Carte geologique de l'ouest du Cameroun et de l'Adamaoua, ORSTOM, 1975.

Le Maréchal, A.: Géologie et géochimie des sources thermominérales du Cameroun, Orstom, 1976.

Li, G., Hartmann, J., Derry, L. A., West, A. J., You, C.-F., Long, X., Zhan, T., Li, L., Li, G., Qiu, W., Li, T., Liu, L., Chen, Y., Ji, J., Zhao, L., and Chen, J.: Temperature dependence of basalt weathering, Earth and Planetary Science Letters, 443, 59-69, http://dx.doi.org/10.1016/j.epsl.2016.03.015, 2016.

Louvat, P., and Allègre, C. J.: Present denudation rates on the island of Reunion determined by river geochemistry: basalt weathering and mass budget between chemical and mechanical erosions, Geochimica et Cosmochimica Acta, 61, 3645-3669, 1997.

Moore, R. B.: Volcanic geology and eruption frequency, São Miguel, Azores, Bulletin of Volcanology, 52, 602-614, 1990.

Nehlig, P., Quinquis, J., Bucelle, M., and Odon, O.: Carte géologique de la Réunion, BRGM, Bur. de Rech. Geol. et Min., Orleans, France, 2006.

Paone, A., and Yun, S.-H.: Pyroclastic Density Current Hazards at the Baekdusan Volcano, Korea: Analyses of Several Scenarios from a Small-Case to the Worst-Case Colossal Eruption, in: Updates in Volcanology-From Volcano Modelling to Volcano Geology, InTech, 2016.

Price, R., McCulloch, M., Smith, I., and Stewart, R.: Pb-Nd-Sr isotopic compositions and trace element characteristics of young volcanic rocks from Egmont Volcano and comparisons with basalts and andesites from the Taupo Volcanic Zone, New Zealand, Geochimica et cosmochimica acta, 56, 941-953, 1992.

Raymond, O. L., Liu, S., Gallagher, R., Highet, L. M., and Zhang, W.: Surface Geology of Australia, 1:1 million scale, dataset 2012 edition, Commonwealth of Australia (Geoscience Australia), Canberra, 2012.

Romero-Mujalli, G., Hartmann, J., and Börker, J.: Temperature and CO2 dependency of global carbonate weathering fluxes – Implications for future carbonate weathering research, Chemical Geology, https://doi.org/10.1016/j.chemgeo.2018.08.010, 2018.

Smets, B., Wauthier, C., and d'Oreye, N.: A new map of the lava flow field of Nyamulagira (DR Congo) from satellite imagery, Journal of African Earth Sciences, 58, 778-786, 2010.

Soller, D. R., Reheis, M. C., Garrity, C. P., and Van Sistine, D. R.: Map database for surficial materials in the conterminous United States, US Geological Survey Data Series, 425, 2009.

Stearns, H. T., and Macdonald, G. A.: Geology and ground-water resources of the island of Hawaii, Honolulu Advertising, 1946.

Tefera, M., Chernet, T., and Haro, W.: Geological Map of Ethiopia, Ministry of Mines, Geological Survey of Ethiopia, GSE, Addis Ababa, Ethiopia, 1996.